The Ascent of 3D X-ray Microscopy in the Laboratory

Arno P. Merkle* and Jeff Gelb
Xradia Inc., 4385 Hopyard Rd. Ste. 100, Pleasanton, CA 94588
*amerkle@xradia.com

Introduction

X rays are universally valued for their ability to penetrate opaque objects. It is only within the past few decades that their short wavelengths have also been exploited to provide 3D imaging of the objects' interiors with resolution well beyond that of light microscopy (LM) in a wide variety of applications. This article explores X-ray imaging as a quantitative sub-micron nanoscale microscopy technique, and specifically its emergent role within the context of the central microscopy laboratory.

X-ray microscopy (XRM) provides non-destructive 3D imaging capabilities on specimens across a range of length scales, observing features with sizes spanning from nanometers to millimeters. Recent developments, inspired by results from dedicated synchrotron sources, have incorporated a number of X-ray optical elements that have driven resolution and contrast to levels previously unachievable by conventional X-ray computed tomography (CT) instrumentation [1]. Furthermore, the non-destructive imaging capability of high-resolution XRM provides unique opportunities to study samples in their native environments (*in situ*) and to quantify how their microstructures evolve over time. These combined characteristics have motivated increased correlative characterization alongside conventional central microscopy laboratory resources, including scanning electron microscopy (SEM), focused ion beam SEM (FIB/SEM), transmission electron microscopy (TEM), light microscopy, and scanning probe microscopy.

X-ray Tomography and Microscopy

Micro-computed tomography (μCT) is an established technique in a number of forms for non-destructively imaging objects in 3D and 4D (evolution over time). However, μCT, as an *optic-free* technique, is subject to trade-offs between sample size and achievable spatial resolution. Total spatial resolution, d_{total}, is a convolution of detector pixel size (r_D), X-ray spot size (S), geometric magnification (M), and the source-to-object and object-to-detector distances (r_{so} and r_{od}, respectively) [1]:

$$d_{\text{total}} = \frac{\sqrt{r_D^2 + \left(S\frac{r_{od}}{r_{so}}\right)^2}}{M} \quad (1)$$

In order to maximize spatial resolution using traditional X-ray detection systems, the conventional μCT approach relies on maximizing geometric magnification [1–2]. Geometric magnification, however, is also a function of the source-to-object and object-to-detector distances, respectively, as shown below [1]:

$$M = \frac{r_{so} + r_{od}}{r_{so}} \quad (2)$$

Thus, in order to maximize geometric magnification, the source-to-object distance must be made very small, limiting the working distance available for high-resolution analysis. As a result, high-resolution imaging of larger samples is not possible; this prohibits high-resolution studies of specimens in chambers intended for *in-situ* experimentation [1–2].

XRM in the laboratory was born from developments in the synchrotron community over the past few decades. Synchrotron facilities across the world continue to push the limits of tomographic imaging in temporal, spatial, and energy resolution [3–10], and laboratory systems are now benefiting from this fertile "proving ground" for new detector and focusing optic technologies [2, 10].

In today's central microscopy laboratory, two basic XRM architectures exist: sub-micron XRM and nanoscale XRM. The following sections will outline their architectures and survey their applications across disciplines.

Two Laboratory-based X-ray Microscopes

Sub-micron XRM. Sub-micron 3D XRM incorporates advanced detection optics, developed at synchrotron facilities over the past decades, coupled with high-energy polychromatic laboratory X-ray sources. By integrating an imaging detector with sufficiently small and tunable pixel size, the standard trade-off of sample size vs. resolution found in the conventional laboratory micro-CT has been improved [1–2]. This permits high-resolution analysis on larger samples and those encapsulated in experimental apparatuses using the technique of local tomography [11]. A two-stage magnification approach (Figure 1) leads to an expanded working distance (Figure 2). The Xradia VersaXRM uses a detector pixel size down to <150 nm to reliably produce spatial resolutions <700 nm on samples several millimeters in size or at working distances measured in the several tens of millimeters [2]. In addition, as a result of small effective pixel dimensions and tunable detector and source positions, propagation phase contrast can effectively highlight interfaces in samples that exhibit low absorption contrast.

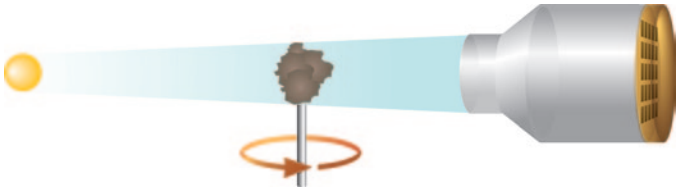

Figure 1: Sub-micron X-ray microscope optical architecture. Magnification is achieved through a combination of geometric (sample, source, detector placement) and optical (post-sample, variable scintillator-lens-CCD coupling) methods.

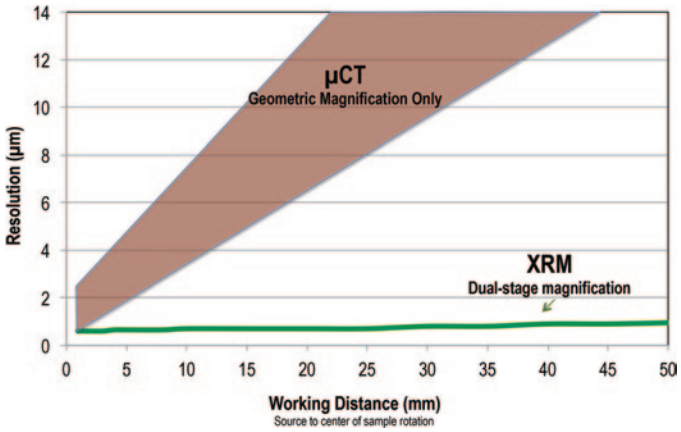

Figure 2: Spatial resolution d_{total} (not voxel size or detectability) as a function of working distance, plotted schematically for conventional μCT and XRM. With post-sample focusing optics, XRM is able to maintain sub-micrometer resolution throughout a range of working distances. Working distance is typically dictated by sample size, geometry, and often by *in-situ* sample stage dimensions.

Nanoscale XRM. Although the sub-micron XRM approach described above is suitable for spatial resolutions into the several hundreds of nanometers and practical voxel sizes (3D analog to 2D pixels, see Figure 3) on the order of 100–200 nm, there is an emerging field of nanoscale XRM that extends voxel sizes (and resolution) down by an order of magnitude.

By incorporating X-ray focusing lenses, laboratory nanoscale XRMs are now able to achieve spatial resolutions down to the tens of nanometers [1–7]. This is made possible largely through the use of Fresnel zone plates, which are diffractive imaging lenses capable of focusing X-ray radiation. The achievable resolution using Fresnel zone plate X-ray optics is determined primarily by the parameters of the zone plate itself; lenses manufactured with finer radial feature sizes increase the maximum achievable XRM resolution.

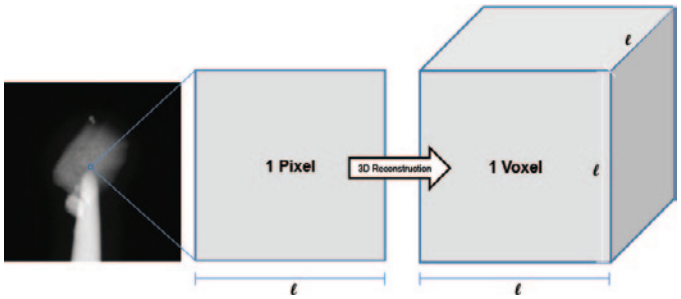

Figure 3: Relationship of pixel size in the sample to voxel size in the 3D reconstructed image.

Analogous to typical light microscopes and TEMs, objective lenses in the nanoscale XRM instrument focus and magnify the object onto a detector in the image plane [1]. The Xradia UltraXRM-L200 system (Figure 4) is based on this geometry and provides laboratory access to 3D and 4D XRM down to about 50 nm spatial resolution, with ultimate voxel sizes down to 16 nm and fields of view up to 65 μm [1–2]. Resolution at this length scale, combined with the intrinsically non-destructive nature of X-ray imaging, is enabling a new class of functional materials science, providing nondestructive access to a wealth of microstructural information [2, 12]. At these length scales, there is reasonable overlap and synergy with emerging 3D FIB-SEM techniques [13]. Nanoscale XRM can study the 3D evolution of a particular microstructure over time (4D) and then pass the sample with a defined coordinate system downstream to the FIB-SEM for final complementary analysis (imaging and spectroscopy, 2D or 3D).

Materials Science Applications

Within the central microscopy laboratory, materials science applications represent a diverse array of material types and sample compositions. Often, materials exhibit changes in microstructure when exposed to different environments (for example, high temperature or pressure conditions), and systematic characterization of this evolution is a challenging task. Using 4D XRM across the millimeter- to nanometer-length scales, a wide range of meso- to micro-structural features may be studied.

Evolution of structure in energy storage materials. The ubiquity of portable electronics coupled with increased worldwide interest in hybrid- and fully electric vehicles has lead to a dramatic increase in electrochemical energy storage device research in recent years. In the case of batteries, the devices are typically supported by porous microstructures within both the anode and cathode regions. The geometries of these pore networks have a significant impact on the charge capacity and output performance of the final battery cells, so characterizing and optimizing the networks is of critical importance to cell development [14].

Using XRM, pore networks may be characterized in 3D with sufficient resolution to obtain fine details that impact cell performance. To understand the observed features at each length scale, the VersaXRM can provide sufficient resolution

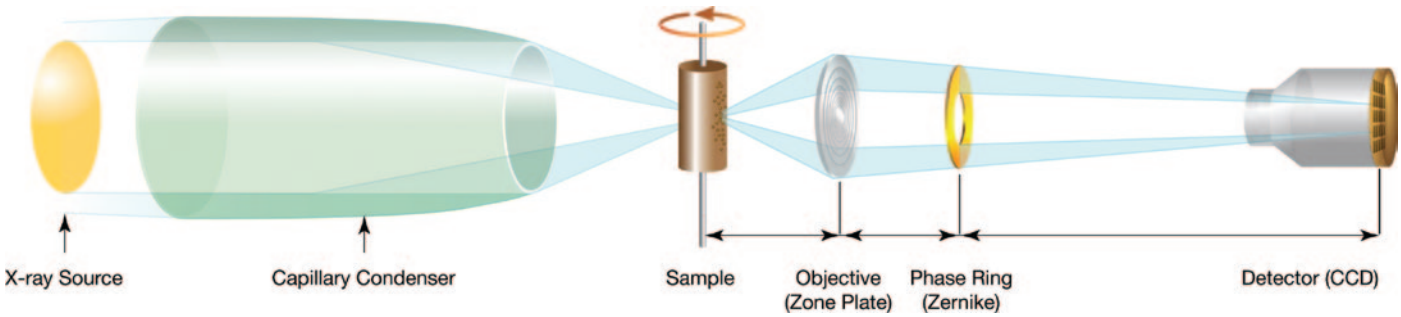

Figure 4: Schematic of the UltraXRM-L200 for nanoscale XRM. A quasi-monochromatic 8 keV illumination passes through the following components: a highly efficient capillary condenser, the sample, a Fresnel zone plate objective lens, an (optional) phase ring (Zernike phase contrast), and a lens-coupled CCD detector.

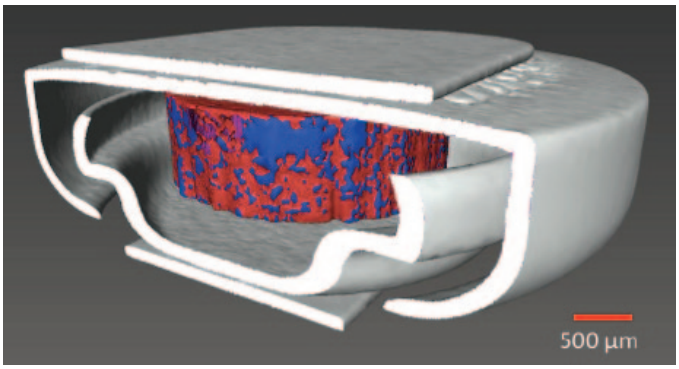

Figure 5: Lithium ion coin cell battery (~5 mm diameter) imaged with sub-micron XRM. Electrode materials may be segmented from the electrolyte to study the microstructural effect of charge cycles on degradation mechanisms [2].

to characterize bulk porosity within electrode microstructures; furthermore, the UltraXRM can measure precise pore geometries and particle surface area-to-volume ratios [15].

The ability of XRM to non-destructively measure battery electrode microstructures lends itself naturally to 4D and *in situ* charge-discharge experiments. The dynamic nature of these devices suggests that microstructural evolution is an important consideration [8, 16]. Nanoscale XRM has been demonstrated to provide unique insight into the evolution of novel electrode compositions that explain electrochemically observed functionality; to date, these experiments have been carried out *in situ* and *in operando* [17–18]. The sub-micron 4D technique enabled by the VersaXRM also has shown promise for evaluation of commercially packaged cells (Figure 5), allowing a true characterization of the 3D microstructure dynamics on a real-world sample under actual operating conditions [2]. Developing the correlation of microstructure to operational conditions may greatly speed up the process of battery innovation.

***In-situ* and 4D characterization.** XRM is particularly well suited for acquiring 3D microstructural information from samples that incrementally undergo change as a result of external influences (mechanical, thermal, electrical, etc.). Studies including compression of structural materials, crack propagation, biasing, heating, and corrosion all present opportunities to quantify the 3D distribution of defects and microstructural changes on the same sample region nondestructively. This avoids the requirements imposed by the destructive techniques of collecting statistical ensembles from varying initial starting conditions. One primary motivation of materials science is to understand materials structure, growth, and failure mechanisms at a sufficient level so that computer models may be used to computationally predict lifetime and performance. One such example (Figure 6) shows a eutectic alloy imaged with both nanoscale and submicron optics, non-destructively, with the intent to image at different growth or solidification conditions. Several studies, including polymer foam compression work, have taken advantage of the ability to output an accurate mesh from a 3D XRM acquisition, place it into a computational model (finite element, fluid dynamics, etc.), and iterate both experiment and model in tandem [19]. It is this improved research efficiency at the sub-micron level that will allow computational materials science to flourish in the coming years. XRM also stands to gain from correlative techniques, whereby the experimental results may be simultaneously validated and expanded through the combination of multiple modalities. Some initial results have been demonstrated that combine XRM and electron microscopy (EM), particularly for work on molecularly imprinted polymers (MIPs) [8, 10, 12].

Porous polymers for fuel cells. Nanoscale XRM has been employed both at the synchrotron [8–10] and in the laboratory [13] to non-destructively quantify the structure of fuel cell electrode materials under a variety of conditions. At the synchrotron, studies have sought understanding of solid oxide fuel cell materials as a function of thermal cycling using *ex-situ* laboratory heaters and *in-situ* heating elements. The goals of such experiments are to quantify the nanoscale microstructure of the same specimen as a function of the external environment; then to perform correlative studies downstream with the SEM, FIB/SEM, or TEM; and finally to compare the results with modeling through finite element method (FEM) and computational fluid dynamics (CFD) approaches.

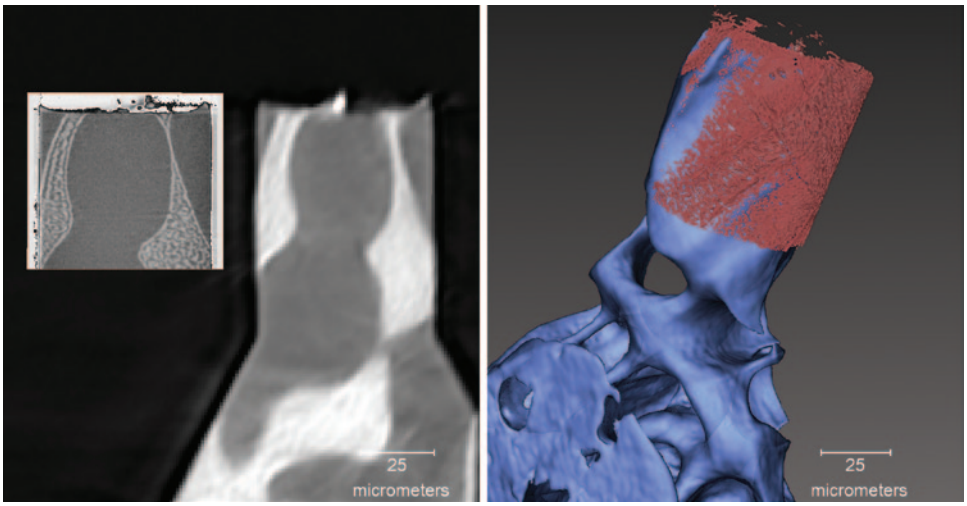

Figure 6: Multiscale image of a Al- 7 at.% Cu eutectic imaged using both the MicroXCT-200 and the UltraXRM-L200. 2D virtual slices on the left (inset: UltraXRM-L200) and segmented volumes on the right. Images courtesy of Brian Patterson, Los Alamos National Laboratory.

Laboratory nanoscale XRM studies on polymer electrolyte fuel cell (PEFC) electrode materials have recently demonstrated the application of large-volume 3D characterization of both pore size and particle agglomerate size distributions, each on the order of a few hundred nanometers [12, 20]. Predicted performance of PEFCs can vary greatly and differ by up to 70% if homogeneous agglomerate size distributions are assumed in the models (Figure 7). This work, performed on the UltraXRM-L200, shows promise for quantifying the agglomerate size and shape distributions, as a function of humidity and

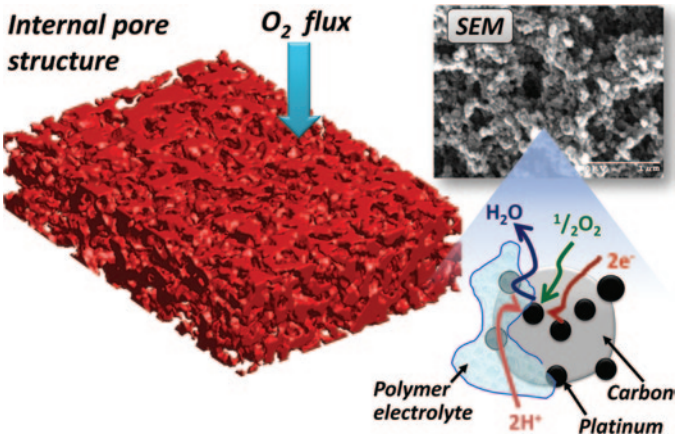

Figure 7: Laboratory-based nanoscale XRM (UltraXRM-L200) used to characterize polymer electrolyte fuel cell (PEFC) electrode materials (left) for fuel cells. Accurate distributions of particle agglomerate sizes and pore dimensions on the order of a few hundred nanometers are needed to feed into models that predict performance. The 3D image volume above is 1.5 µm × 4.5 µm × 7 µm. Sample and image courtesy of Shawn Litster and William Epting, Carnegie Mellon University.

other environmental factors, to accurately understand the microstructural changes associated with PEFC performance. At the same time, experimental cross-validation of XRM and TEM enhances confidence in the experimental conclusions (the correlative microscopy approach).

Life Science Applications

The research topics currently being carried out by XRM in the life sciences are diverse. The ability to provide high contrast (tunable absorption and phase contrast) for samples of low-*Z* materials has opened up a number of important new pathways for biomedical and basic biology research, including studies in developmental biology, soft-tissue, agriculture, hard-tissue, bio-engineered materials, and scaffold materials for tissue engineering.

Immunostaining has become an important tool for biological and biomedical research, providing information on the distribution of gene products such as proteins and ribonucleic acids. This has been developed primarily through light microscopy-based techniques, including serial sectioning histology and optical projection tomography (OPT). However, because of the limited penetration depth of visible light, these techniques are often limited to either small samples ranging from tens to hundreds of micrometers or to coarser resolutions (>10 µm). Sub-micron XRM has been successful in quantitatively characterizing small mammalian embryos at a spatial resolution of <1 µm (<200 nm pixel) in order to spatially visualize individual cell bodies [21].

Correlative microscopy methods continue to occupy a central theme behind imaging developments within the life science microscopy community. Because it is fully acknowledged that no single microscopy technique can provide a complete picture of a specimen, the challenge turns to finding practical methods of localizing the same feature in multiple microscopes [22].

In the field of neuroscience, there is interest in creating complete neural network maps of brain tissue down to individual synaptic junctions in order to extend our understanding of neural function and disease. The need for this information across length scales in 3D down to the nanometer length scale has spawned the development of high-throughput 3D electron microscopy (3DEM) techniques, based on TEM and SEM methods that incorporate either physical sectioning via cutting (ultra-microtome) or ion abrasion (FIB-SEM). The 3DEM concept uniquely provides high-quality ultrastructure information to complement functional and/or dynamic (4D) information from LM. While resolution in 3DEM is at the nanometer-level laterally and several nanometers vertically, the method still requires standard chemical fixation methods and heavy-metal staining, often after the sample has been visualized in LM. However, these 3DEM techniques can prosper only if one finds ways to avoid common constraints including long acquisition times (or small sample volumes), sensitivity to sample preparation, and inefficiencies in locating regions of interest (buried subsurface features).

Most electron microscope manufacturers have launched commercial correlative microscopy solutions within the past few years to navigate between and correlate LM and EM images via software and hardware methods. A remaining challenge here is to improve experiment efficiency when using multiple modalities to image the same sample. However, it is well known that sample preparation requirements can be radically different for LM compared to EM. Chemical fixation and heavy-metal staining procedures that are used to optimize EM contrast have the side effects of rendering previously transparent samples opaque in the light microscope as well as possibly modifying the bulk 3D microstructure. Therefore, in order to successfully navigate to a subsurface feature, the National Center for Microscopy and Imaging Research (NCMIR) is using XRM as a bridge between LM and EM. XRM has the potential to fill this gap by exhibiting sufficient resolution and contrast on classically prepared stained EM tissue samples.

3D imaging of brain tissue. Figure 8 shows an early example from an ongoing collaboration between Xradia and

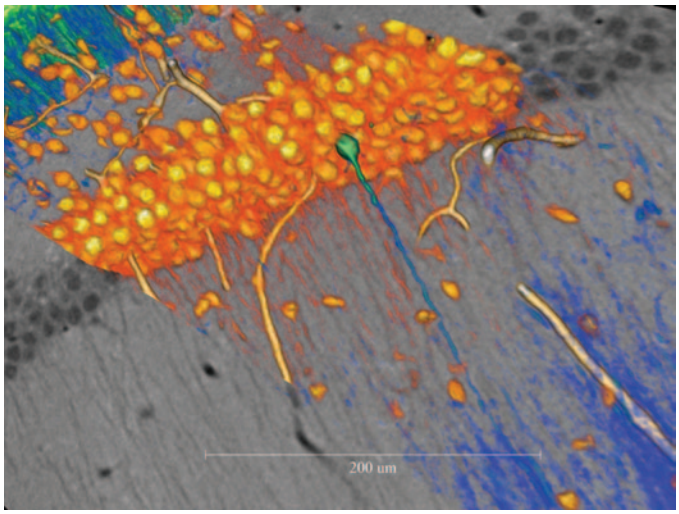

Figure 8: Sub-micron XRM image (VersaXRM) of EM-stained mammalian brain tissue from a section ~100 µm thick. The 3D reconstructed volume rendering (color, visualized with VSG's Avizo Fire 7) is overlaid on one 2D virtual slice (grayscale image). Individual neuron cells are resolved, showing dendrites. A single diaminobenzidine-labeled neuron can be identified (green). This example is from work being carried out by the National Center for Microscopy and Imaging Research (NCMIR) at the University of California at San Diego in collaboration with Xradia.

NCMIR using the VersaXRM-500 to image mammalian brain tissue. This slice of mouse brain was fixed, stained, and embedded for EM imaging after LM investigation. X-ray absorption contrast is clearly able to detect individual neural cell bodies and dendrites in three dimensions. Furthermore, a single cell was labeled and successfully differentiated in the XRM absorption image (rendered in green in the 3D overlay). Such 3D XRM datasets can be used to provide the requisite 3D information to guide subsequent EM data acquisition. Nanoscale XRM also has imaged sub-cellular details in frozen hydrated specimens through the use of soft X rays ("water window") with both synchrotron and laboratory sources [23].

Geoscience Applications

Driven by applications such as solutions for CO_2 capture/sequestration and optimizations of oil and gas extraction efficiencies, the complexity of geological formations is becoming of interest to academic and industrial researchers alike. Of the many modalities currently in use, XRM is at the cornerstone of modern geological investigation techniques, owing to its non-destructive multi-length scale 3D imaging capabilities, as well as its flexibility for handling *in-situ* flow cells.

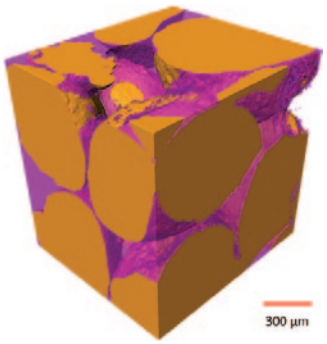

Figure 9: Sub-micron XRM of partially water-saturated silica granules. Water (purple), pores (not shaded), and silica (orange) are segmented without the use of additional contrast agents for the liquid. Sample courtesy of F. Kim and D. Penumadu, University of Tennessee at Knoxville.

Oil and gas extraction. Geological microstructures consist of complex 3D pore pathways in matrices that are often highly heterogeneous (Figure 9). Within industrial oil and gas extraction research, understanding the 3D pathways and localized compositions helps to provide an estimate of potential yield for a prospective drilling site. The complexity of rock microstructure is a critical factor in performing analysis on many of the conventional sandstone and carbonate reservoir rocks, but it becomes especially important for modern unconventional sources, such as shale. With that importance, however, comes a challenge: the pore sizes are also highly heterogeneous, expanding into large vugs in some locations and tapering to small throats in others. Traditional pore analysis techniques, such as physically measuring the rate of fluid flow, are impeded by the pore throats, and it may take a long time to analyze enough specimens to achieve a result that is sufficiently statistically significant to characterize the well site.

The role of 3D microscopy in the geological and reservoir engineering laboratory is to gain a complete picture of the rock microstructure in a fraction of the time needed for physical fluid flow measurements. Using the modern technique of digital core analysis (DCA), pore networks may be virtually extracted and subsequently coupled with novel approaches in computer simulations to model the fluid flow through the specimen. It is here that XRM has proven especially valuable. The multi-length scale capabilities enable observation of a complete core volume, with millimeter to nanometer precision, for developing comprehensive models of fluid transport pathways. Large core samples may be surveyed with a technique such as industrial CT, from which certain regions may be identified for micrometer-scale analysis using an XRM platform such as the VersaXRM. From these volumes, regions for even higher resolution analysis may be identified (for example, small pore throats), and the UltraXRM may be employed to produce reliable models of those features down to tens of nanometers in size [11, 24]. The specimen may be subsequently investigated with a destructive technique, such as flat-polished section analysis by SEM, to supplement the results with information on the single nanometer length scale.

In addition to the multi-length scale characterization approach, XRM is also advantageous for its ability to handle *in-situ* experimental set-ups, such as flow cells. By physically flowing fluid through a geological specimen and simultaneously measuring the fluid's position relative to the total pore space, quantities such as capillary pressure may be measured. Modern flow cells also enable the variation of input pressure, enabling insight into local fluid flow phenomena. This enables experimental validation of flow models for high-precision results [25].

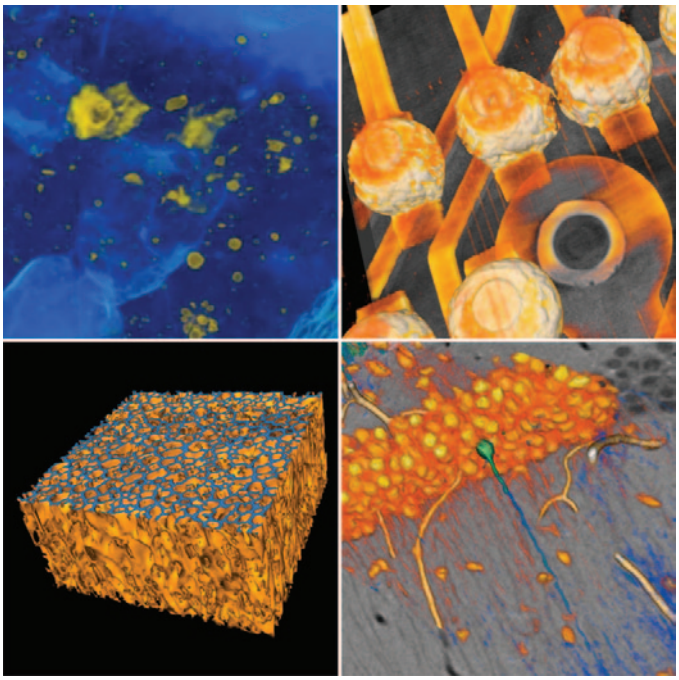

Figure 10: Winning entries in four categories from the 2012 Xradia Image Contest. **Geology (upper left):** carbonaceous chondrite meteorite that landed on April 22, 2012, at Sutter's Mill, CA, imaged with an Xradia MicroXCT-200. Iron or iron sufide (yellow) in a matrix (blue) containing Mg, Si, Al, Ca, C, and O. Image width = 9 mm. Courtesy of Prof. Qing-Zhu Yin, UC Davis. **Electronics (upper right):** microelectronic device with short circuit between two bumps imaged with Xradia VersaXRM-500. Image width = 600 µm. Courtesy of S.T. Crolles. **Materials Science (lower left):** soft porous polymer with urethane backbone (blue) imaged *in situ* with Xradia Versa-XRM-500 under varying temperature and compression. Image width = 200 µm. Courtesy of National Chemical Laboratories, India. **Life Science (lower right):** mammalian brain tissue section showing individual neuron cells imaged with Xradia VersaXRM-500 (see Figure 8). Image width = 260 µm. Courtesy of the National Center for Microscopy and Imaging Research at UC San Diego.

Discussion

The range of imaging applications for X-ray microscopy can be appreciated from a small sampling of the entries in the 2012 Xradia Image Contest. The winning entries in four categories are shown in Figure 10. The top two images show X-ray images of hard materials containing at least some dense constituents. The lower two images in the figure show X-ray images of low-density soft materials. The pseudo-colors in these images were chosen to highlight features of different density. All four images contain information that could not easily be obtained by light or electron microscopy.

Conclusion

This review of laboratory-based 3D XRM examined the emergence of 3D XRM as a complementary non-destructive imaging technique for the general microscopy laboratory. The technique is useful across a wide spectrum of sample types and can characterize samples in their native environments. Looking toward the future, 3D XRM is likely to develop into a standard characterization step to be used as a precursor to other techniques such as TEM and SEM. LM and EM laboratories are expected to benefit greatly from 3D XRM datasets that can facilitate efficient navigation to a particular defect or region of interest. The 3D XRM method also can non-destructively follow the evolution of a microstructure in response to environmental conditions or stressors, providing 4D characterization.

References

[1] A Tkachuk, F Duewer, H Cui, M Feser, S Wang, and W Yun, *Z Kristallogr* 222 (2007) 650–55.
[2] J Gelb, *Ad Mat Proc*, 170(10) (2012) 14–18.
[3] Q Yuan, K Zhang, Y Hong, W Huang, K Gao, Z Wang, P Zhu, J Gelb, A Tkachuk, M Feser, W Yun, and Z Wu, *J Synch Rad* 19(6) (2012) 1021–28.
[4] J Wang, Y-C K Chen, Q Yuan, A Tkachuk, C Erdonmez et. al., *Appl Phys Lett* 100(14) (2012) 143107–10.
[5] JC Andrews, S Brennan, C Patty, K Luening, P Pianetta, E Almeida, MCH van der Muelen, M Feser, J Gelb, J Rudati, A Tkachuk, and W Yun, *Synch Rad News* 21(3) (2008) 17–26.
[6] Y Tian, W Li, J Chen, L Liu, G Liu, A Tkachuk, J Tian, Y Xiong, J Gelb, G Hsu, and W Yun, *Rev Sci Inst* 79(10) (2008) 103708.
[7] YS Chu, JM Yi, F De Carlo, Q Shen, W-K Lee, HJ Wu, CL Wang, JY Wang, CJ Liu, CH Wang, SR Wu, CC Chien, Y Hwu, A Tkachuk, W Yun, M Feser, KS Liang, CS Yang, JH Je, and G Margaritondo, *Appl Phys Lett* 92 (2008) 103119–21.
[8] PR Shearing, RS Bradley, J Gelb, SN Lee, A Atkinson, PJ Withers, and NP Brandon, *Electrochem Solid St* 14(10) (2011) B117–20.
[9] Y Guan, Y Gong, W Li, J Gelb, L Zhang, G Liu, X Zhang, X Song, C Xia, Y Xiong, H Wang, Z Wu, and Y Tian, *J Power Sources* 196(24) (2011) 10601–05.
[10] PR Shearing, RS Bradley, J Gelb, F Tariq, PJ Withers, and NP Brandon, *Solid State Ionics* 216 (2012) 69–72.
[11] J Gelb, S Roth, H Dong, D Li, A Gu, S Yun, and W Yun, *Proc SCA* (2012) SCA2012–59.
[12] W Epting, J Gelb, and S Litster, *Adv Func Mat* 22(3) (2011) 555–60.
[13] PR Shearing, J Gelb, and NP Brandon, *J Eur Ceram Soc* 30 (2010) 1809–14.
[14] PR Shearing, NP Brandon, J Gelb, R Bradley, PJ Withers, AJ Marquis, S Cooper, and SJ Harris, *J Electrochem Soc* 159(7) (2012) A1023–27.
[15] D Kehrwald, PR Shearing, NP Brandon, PK Sinha, and SJ Harris, *J Electrochem Soc* 158(12) (2011) A1393–99.
[16] H-R Jhong, FR Brushett, L Yin, D Stevenson, and PJA Kenis, *J Electrochem Soc.* 159(3) (2012) B292–98.
[17] S-C Chao, Y-C Yen, Y-F Song, Y-M Chen, H-C Wu, and N-L Wu, *Electrochem Comm* 12 (2010) 234–237.
[18] J Nelson, S Misra, Y Yang, A Jackson, Y Liu, H Wang, H Dai, JC Andrews, Y Cui, and MF Toney, *J Am Chem Soc* 134 (2012) 6337–43.
[19] BM Patterson, K Henderson, Z Smith, D Zhang, and P Giguere, *Microscopy & Analysis* 26(2) (2012) S4–S7.
[20] S Litster, K Hess, W Epting, and J Gelb, *ECS Trans* 41(1) (2011) 409–18.
[21] B Metscher, *Dev Dyn* 238 (2009) 632–40.
[22] J Priester, Y Ge, RE Mielke, AM Horst, SC Moritz, K Espinosa, J Gelb, SL Walker, RM Nisbet, Y-J An, JP Schimel, RG Palmer, JA Hernandez-Viezcas, L Zhao, JL Gardea-Torresdey, and PA Holden, *PNAS* 109(37) (2012) E2451–56.
[23] D Carlson, J Evans, and J Gelb, *Micros Microanal*, in press.
[24] FH Kim, D Penumadu, A Gu, S Yun, and J Gelb, *Proc SCA* (2012) SCA2012–61.
[25] S Roth, D Li, H Dong, and MJ Blunt, *Proc SCA* (2012) SCA2012–02.

MT